Coupling technique for efficient interfacing between silica waveguides and planar photonic crystal circuits

Yuan-Fong Chau, Tzong-Jer Yang, and Win-Der Lee

We describe a two-step-size tapered structure with one defect pair that can markedly enhance the coupling efficiency at the entrance and exit terminals of a planar photonic crystal (PPC) waveguide. PPC waveguides are composed of circular dielectric rods set in two-dimensional square lattices. On the basis of our simulations, we found that the optimized scheme maximizes the power transmission above 90% at a wavelength of 1.55 μm. Besides, one can control the central frequency for optical communications by determining this defect configuration in an optimization procedure. Moreover, by properly adjusting the defect radii in PPC tapers, one can use the PPC circuit as a good reflector.

OCIS codes: 230.3120, 260.0260, 260.2110.

1. Introduction

Photonic crystal (PC) waveguides are expected to play an important role in the development of highly integrated optical circuits (IOCs). Owing to its relevant features such as ease of manufacture, compactness, and small size, the planar photonic crystal (PPC) has attracted great interest for development in microscale IOCs. PPCs have been designed to simplify manufacturing.[1] It has been predicted and shown that light can be efficiently guided through line defects in PPC structures. However, propagation losses that arise from coupling integrated dielectric waveguides to PPC waveguides are traditionally high. As the coupling process (either into or out of a PC waveguide) is essentially a scattering phenomenon,[2] one might imagine that modification of the termination surface morphology of the waveguide would induce a large change in the coupling behavior and that, with careful design, the coupling efficiency could reach a large optimum value. Thus it is necessary to develop reliable PPC circuits to minimize coupling losses between conventional silica waveguides (SWGs) and PPC waveguides. Several coupling structures and techniques have been proposed.[3–8] Among the proposed methods, one of the most promising is the use of PPC tapers,[7,8] mainly because of their small coupling length (<5 μm) and high coupling efficiencies achieved over a large frequency range with transmission peaks exceeding 80% at localized frequencies. However, these structures (as described in Refs. 3–8) are sensitive to manufacturing inaccuracies. The experimental achievement of such structures is much more difficult because many defect pairs must be used and one must vary the rod size to achieve an artificial material with an effective gradient index and adiabatic mode transformation.

These active issues represent a challenge that must be met if PC waveguides are to be used in IOCs. We need to find a way to couple light efficiently at the entrance and exit terminals of lines of defects in photonic bandgap materials. Because the physics of traditional index guiding and of photonic bandgap guiding are different, coupling light into and out of PC waveguides is far from a trivial exercise. There can be substantial reflection and scattering from PC waveguide ends that will adversely affect the outcome of transmission measurements. This is a considerable drawback if one is to test novel PC devices efficiently. To overcome this limitation, one needs an efficient waveguide junction design. A novel coupling technique based on setting a single localized defect within a 0.5-μm-long PPC tapered waveguide structure in a triangular lattice of circular dielectric rods in a silica background was proposed,[9] that significantly improves the transmission results by use of

Yuan-fong Chau (yfchau@mail.apol.com.tw) and Win-Der Lee are with the Department of Electrical Engineering, Lee-Ming Institute of Technology, Taipei 30050, Taiwan. Tzong-Jer Yang is with the Department of Electrophysics, National Chiao Tung University, Hsinchu, Taiwan.

Received 8 April 2004; revised manuscript received 8 September 2004; accepted 12 September 2004

0003-6935/04/366656-08$15.00/0

only a conventional (one-step-size lattice constant) PPC taper.[6] However, the transmission measured inside the PPC waveguide reached an average value of only 62%, and the transmission efficiency decreased as the width of the SWG increased. Note that a measurement point set inside a PPC waveguide cannot represent the actual transmission. Besides, wider PPC tapers are required for efficient mode-profile matching to wider dielectric waveguides.

Motivated by the previous publications cited above and addressing the changes suggested in this paper, we show that the proposed coupling technique can also be employed with wider PPC tapers but that in such a case a pair of defects at symmetrical positions in the PPC tapers must be designed for the required PPC taper to have maximum transmission efficiency. The introduction of localized defect pairs is investigated, as well as their effects on the frequency transmission spectra when couples at the entrance and exit sides of a PPC waveguide are considered. By proper defect mode matching at the interface between a SWG and a PPC waveguide, which will significantly improve the transmission efficiency compared with that of a butt-coupled waveguide, a conventional PPC taper without defects and two-step-size lattice constant PPC tapers without and with defects will be achieved.

2. Structure and Coupling Technique

The practical use of a SWG and PPC tapers for coupling IOCs is limited if there are no good approaches to coupling light into them efficiently. It is our aim in this paper to present a high-efficiency technique for coupling a SWG and PPC waveguides in the form of square lattice of dielectric rods surrounded by a homogeneous silica medium. Triangular lattices have been reported.[7–9] To the best of our knowledge, coupling into this structure has never been thoroughly investigated. In this paper we restrict our attention to waveguide junctions for this type of waveguide, as they have been the focus of recent theoretical and experimental investigations.[10,11] The PPC structure considered here is a two-dimensional (2-D) square array of dielectric rods of lattice constant a surrounded by a homogeneous dielectric medium. The rods have a refractive-index value of 3.45, which corresponds to that of silicon (Si) at 1.55 μm, and a circular cross section of radius $0.2a$. The surrounding medium in the PPC has an index value of 1.45, which corresponds to that of silica (SiO_2) at 1.55 μm. A SWG has dielectric index of 1.45 and width w, and the surrounding dielectric medium is air. This PPC has a large bandgap for TM-polarized waves (i.e., the electric field is oriented in the axis of the rods, where all rods have the same axis). A lattice constant value of 0.465 μm was chosen because the transmitted band is fixed near 1.55 μm. This lattice constant value is equivalent to $a/\lambda = 0.3$ for $\lambda = 1.55$ μm. Such a value is appropriate for transmission at standard optical communication wavelength. For such a lattice constant the

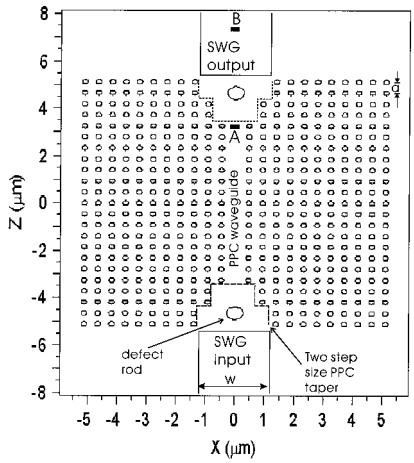

Fig. 1. Schematic view of the structures considered. A 2.4-μm-wide–$4a$-long two-step-size lattice constant PPC taper (where a is the lattice constant) with a radius of defect configuration is introduced into a PPC taper employed to couple light both into and out of a finite-length (15 rows) PPC waveguide from a SWG. The optical power transmitted through the PPC waveguide is measured with two power monitors, one placed inside the waveguide at point A and the other at the output end at point B.

PPC substrate has a PBG range of wavelength in free space from 1.44 to 1.68 μm for TM-polarized waves, calculated by a 2-D plane-wave expansion method.[12] The PPC waveguide is created along direction W1 [one row of dielectric rods removed in the (1 0) direction of the photonic crystal]. We achieve a discrete taper by removing three (W3, three rows of dielectric rods removed in the same direction as W1) and five (W5, five rows of dielectric rods removed in the same direction as W1) rods of the original PPC waveguide to form a two-step-size lattice constant PPC taper, as shown in the areas enclosed by dashed lines in Fig. 1, which neutralize a defect rod to form a cavitylike environment.

As described in Ref. 13, adiabatic transmission in a PPC waveguide may be achieved if it is guaranteed that the operating mode of every-unique feature in the PPC waveguide and the PPC taper is different. Therefore the behavior of these features may be predicted by calculation of independent dispersion diagrams. The dispersion relations for the PPC waveguides shown in Fig. 1 are calculated by the plane-wave expansion method in the frequency domain for given dielectric configurations. We need to identify a supercell with periodic boundary conditions as the computation domain. The supercells' dimensions are set (19, 1, 1), where (19, 1, 1) means numbers of cells in x, y, z directions. The choice of 19 cells in the x direction is essentially a guess. The calculation should be repeated with different-sized supercells to check for convergence. We determine the TM band structures for three different PPC waveguides (W1, W3, and W5) to identify their features that are different from those in conventional waveguides. The results are shown in Fig. 2. The horizontal axis is the wave vector in the direction of

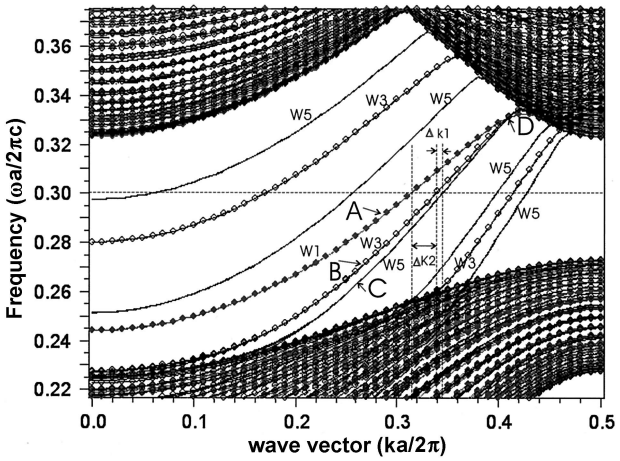

Fig. 2. Dispersion relations for the TM band structures for three (W1, W3 and W5) PPC waveguides in a 2-D square array of dielectric rods of lattice constant a surrounded by a homogeneous dielectric medium, where W1 (W3, W5) is created by removal of one (three, five) rod(s) of the original PPC waveguide. The three modes A, B, and C (arrows) indicate guide modes W1, W3, and W5, respectively.

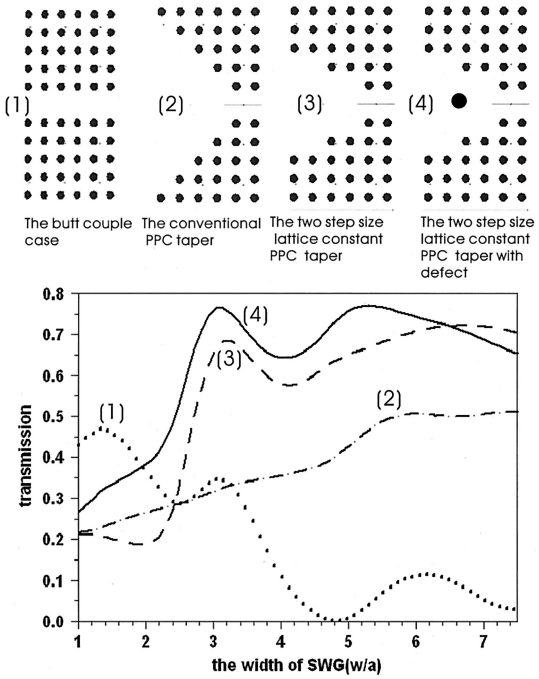

Fig. 3. Normalized transmission spectra as a function of w/a for a wavelength of incident light that corresponds to $\lambda = a/0.3 = 1.55$ μm, where $a = 0.465$ μm, for four cases: (1) a butt-coupled structure; (2) a conventional PPC taper; (3) a two-step-size lattice constant PPC taper without defects; and (4) the same as case (3), except with a defect rod, where the defect radius is $r = 0.3$ μm and defect pairs are located at $(0, -9.7a)$ and $(0, +9.7a)$. The transmitted field is measured at the output end of the SWG (point B) by a power monitor covering the exit of the PPC waveguide as shown in Fig. 1.

the guide, and the band structures are shown in a reduced Brilliouin zone scheme. The modes inside the gap are localized to the row of missing rod. The filled circles (dark gray) in Fig. 2 show the band structure for the guide in the W1 direction. We found a single guide mode inside the bandgap. The electric field of the mode has even symmetry with respect to the mirror plane along the guide axis. The mode itself bears a close resemblance to the fundamental mode of a conventional dielectric waveguide. We made the open circles in Fig. 2 by removing three rows of rods in the W3 direction. There are now three guide modes inside the gap that can again the classified according to their symmetry with respect to the mirror plane along the guide axis. It is generally true that the number of bands inside the bandgap equals the number of rows of rods removed when the guide is created. Analogously, when five rows of rods are removed, we pull up five (solid curves) guide modes at each location k (wave vector) from the dielectric band. In Fig. 2, the filled circles (dark gray) denote the W1 mode, the open circles denote the W3 mode, and the solid curves denote the W5 mode. The three nearby guide modes, A, B, and C, which are modes of W1, W3, and W5, respectively, at the arrows indicated in Fig. 2, are close to each other at normalized frequency $a/\lambda = 0.3$. It can be seen from Fig. 2 that the three modes A, B, and C merge at point D [$k_z = 0.4098$, $(\omega a)/(2\pi c) = 0.3316$]. This means that they are coupled at point D, i.e., that their eigenmodes propagate at the same wave vector. As was stated by Bayindir *et al.*,[14] coupling length $L = a/(2\Delta k)$, where Δk is the difference between two wave vectors at a given normalized frequency. This formula shows that Δk strongly depends on the normalized frequency, implying the splitting of large dispersion. Obviously, the value of L is infinity for coupling of the PPC waveguide when Δk approaches zero, which takes place at point D and gives rise to the merger of the eigenmodes. In Fig. 2 the small value of $\Delta k1$ shows the difference in wave vectors of guide mode B and guide mode C at the same normalized frequency of 0.3. It can be seen that there is a small dispersion split, which implies that the two types of waveguide that form the two-step-size lattice constant PPC taper can couple a light wave easily from W5 to W3 but has some difficulty in coupling the light wave into guide mode A (from W3 to W1) because of the larger value of $\Delta k2$ (the difference of wave vectors between guide mode A and guide mode B at the same normalized frequency of 0.3). Based on the above analysis, note that we have an opportunity to use an optimum defect configuration as a mode-matching trick in the two-step-size lattice constant PPC taper [which we achieve by removing three (W3) and five (W5) rods of the original PPC waveguide] for coupling into the PPC waveguide [by removing one (W1) rod of the original PPC waveguide]. Therefore the proper-mode maybe achieved by setting a defect in the PPC taper when the interfaces between the SWG and PPC waveguides are controlled to prevent an abrupt change in the reflectivity at input–output of resonant cavities.[15,16]

The coupling structure investigated consists of a

PPC taper with a dielectric defect rod as a defect of a different radius. Mode matching is achieved by choice of the optimum defect parameters within the PPC taper. In this paper we describe a special PPC taper structure, i.e. a 2.4-μm-wide/4a-long two-step-size lattice constant PPC taper (where a is the lattice constant, here 1.86 μm). An optimal radius of defect configuration is introduced in the PPC taper to couple light both into and out of a finite-length (15 rows) PPC waveguide, as shown in Fig. 1, from which it may be observed that a SWG guides the input light to a tapered input PPC waveguide passing through the dielectric defect rod. The optical power transmitted through the PPC waveguide is measured by two power monitors, one placed at the exit end of the PPC waveguide (at point A) and the other at the output end of the SWG (at point B), as shown in Fig. 1. The defect rod within the PPC taper has radius r, and its position z_{opt} along the z axis is further optimized to achieve the highest coupling efficiency.

Coupling losses between a conventional SWG and PPC waveguides arise mainly from the mode mismatch derived from the various widths and propagation mechanisms in a SWG and PPC waveguides that decrease the coupling efficiency and increase the reflection losses. To overcome these losses, localized defect pairs are introduced within the 2.4-μm-wide/4a-long two-step-size lattice constant PPC tapers at the entrance and exit terminals of the PPC waveguide that alter the modal properties of the guided mode. Thus one can achieve mode matching by determining the optimum radii of defect pairs as well as the other optimum parameters (the width of the SWG and its relative position within the PPC tapers). An approach is necessary for setting localized defect pairs into PPC tapers owing to the variation of the modal properties along the taper. An optimized study of the proposed coupling technique was made by numerical simulations. This study is aimed at determining the optimum parameter values (width w of the SWG, defect radius r, and relative defect position z_{opt} within the two-step-size lattice constant PPC taper along the z axis at sectional plane $x = 0$) of the structure shown in Fig. 1 to achieve the highest coupling efficiency, i.e., maximum transmission through the PPC waveguide from the light coming from the input end of the SWG to the output end of the SWG.

3. Results and Discussion

Let us first optimize the width of the SWG and the radius of the defect and improve the transmission by optimizing the relative position of the defect that should be placed into the PPC taper. The next method is based on a 2-D finite-difference time-domain algorithm.[17] A grid size of $a/50$ is used in the finite-difference time-domain simulations, and the condition of a perfectly matched layer is considered at (the boundary zone to ensure that there is no backreflection within the limit of the region analyzed,[18] which is terminated by a 0.5-μm width to produce perfectly absorbing boundary conditions. First, the SWGs width (w), the defect position (z_{opt}), and the defect radius (r) have been optimized at the 0.3 (a/λ) normalized frequency located close to 1.55 μm for the lattice value considered. To excite the modeling structure of the input end of the SWG we used a sinusoidal monochromatic continuous wave with normalized power as the light source in the z direction, with a Gaussian transverse field pattern in the x direction. Removing several additional dielectric rows as displayed in the upper part of Fig. 3 creates different shapes of the PPC taper. Figure 3 shows the normalized transmission spectra as functions of w/a for a wavelength of incident light that corresponds to $\lambda = a/0.3 = 1.55$ μm when $a = 0.465$ μm for four cases: (1) a butt-coupled structure; (2) a conventional PPC taper; (3) a two-step-size lattice constant PPC taper without defects; and (4) the same as case (3), except with a defect rod, where there is defect radius of $r = 0.3$ μm and defect pairs are located at $(0, -9.7a)$ and $(0, +9.7a)$. The transmitted field is measured at the output end of the SWG (point B) by a power monitor covering the exit of the PPC waveguide as shown in Fig. 1. The transmission spectra are calculated from the Fourier-transformed time series and normalized with respect to the launched field.

For case (1) of Fig. 3, the transmission of the butt-coupled case oscillates and rises to a maximum transmission of 47% when the SWG's width is 1.34a (623.1 nm) and then descends to zero at width 4.8a (2.232 μm). As the width of the SWG is greater than 1.34a, coupling is inefficient. It is clearly evident that the transmission decreases while the width of the SWG increases owing to backreflection from the various widths and mechanisms between the SWG and the PPC waveguide. One of the reasons for this is the poor mode-profile match between the fundamental modes of the wide dielectric and of the much narrower PPC waveguide. From physical intuition, one might imagine that the tapering structure can help to couple an external signal into a PPC waveguide and also help to couple a guided wave out of the PPC waveguide. For case (2) of Fig. 3, i.e., a conventional PPC taper without defect, the transmission increases while the width of SWG increases, achieving transmission up to a steady value of 50% for a width of the SWG of more than 6a (2.79 μm). As a comparison, case (2) can result in flat [no oscillation shown in case (2) compared with that shown in case (1) of Fig. 3] and higher transmission when the butt-coupled structure is replaced by a conventional PPC taper. This result can offer some hints for designing a high-performance PPC waveguide when the aspect of the taper structure is well designed. As a two-step-size lattice constant PPC taper without a defect [case (3) of Fig. 3] has been adopted, the transmission sharply increases, achieving a transmission of as much as 57% for a SWG width of more than 3.2a (1.49 μm). Because of better mode matching between the SWG and the two-step-size PPC taper, transmission is more efficient than the results shown for cases (1) and (2) of Fig. 3. As was mentioned in Section 2, the

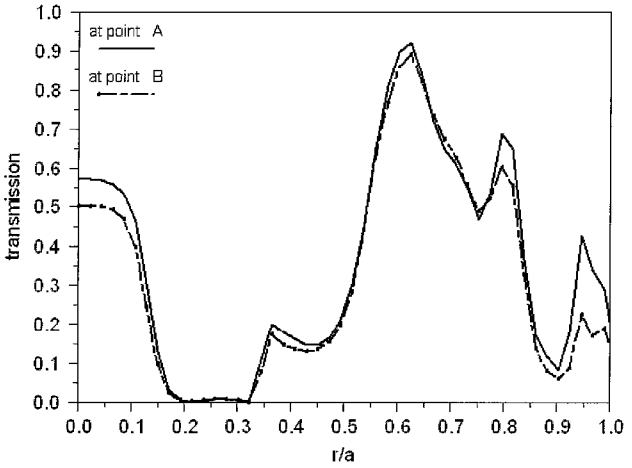

Fig. 4. Normalized transmission spectra as a function of r/a for a wavelength of incident light that corresponds to $\lambda = a/0.3 = 1.55$ μm, for SWG width $w = 2.4$ μm. The defect pairs are located at $(0, -9.7a)$ and $(0, +9.7a)$. The optical power transmitted through the PPC waveguide is measured with two power monitors, one at the exit terminal of the PPC waveguide (point A) and other at the output end of the SWG (point B), as shown in Fig. 1, where a denotes the lattice constant and λ is the wavelength of light in vacuum.

two-step-size lattice constant PPC taper can couple a light wave easily from W5 to W3 but shows some difficulties from W3 to W1. That is, the k mismatch between W3 and W1 must be resolved if the aim of high transmission is to be fulfilled; i.e., the field distributions inside the PPC taper must be change for mode-profile matching between the SWG and the PPC taper to be achieved. Thus, defect pairs set in the entrance and exit terminals of PPC tapers will be key factors in handling the field distributions between the SWG and the PPC taper. It can be seen from case (4) of Fig. 3 that the introduction of defect pairs within the two-step-size lattice constant PPC tapers at the entrance and exit terminals of a PPC waveguide improves the transmission by as much as 64% for a SWG width ranging above $3.1a$ (1.44 μm). Note that the profiles of transmission spectra obtained in cases (3) and (4) are similar for a SWG width ranging from $2.5a$ (1.1625 μm) to $5.4a$ (2.511 μm), which means that defect pairs set in a PPC taper can improve mode impedance matching but not modify the spectra. The optimum SWG widths to achieve the maximum transmission (78%) are $3.17a$ (1.5 μm) and $5.22a$ (2.4 μm). Besides, the wider SWG width increases the transmission shown in case (4) counterintuitively lower than that shown in case (3) for a SWG width above $6.512a$ (3.03 μm). That is, case (4) seems to present a local optimum transmission when the SWG width ranges from $3.1a$ (1.44 μm) to $6.512a$ (3.028 μm). One of the reasons that the SWG width-increases above $6.512a$ is that the light coupling into the PPC waveguide has a lower transmission efficiency because in this case there are many channels into which a wave reflected from the junction can couple.

In Fig. 4 the normalized transmission spectra as functions of r/a for the wavelength of incident light correspond to $\lambda = a/0.3 = 1.55$ μm, where for SWG width $w = 2.4$ μm the defect pairs are located at $(0, -9.7a)$ and $(0, +9.7a)$. The optical power transmitted through the PPC waveguide is measured with two power monitors, one at the exit terminal of the PPC waveguide (point A) and the other at the output end of the SWG (point B), as shown in Fig. 1, where a denotes the lattice constant and λ is the wavelength of light in vacuum. From Fig. 4 it can be seen that the maximum transmission (93% at point A, 90% at point B) is achieved for $r = 0.622a$ (0.289 μm) instead of $r = 0.3$ μm, which is assumed in case (4) of Fig. 3. The way to achieve coupling is to use an interface resonant mode to couple the mode in the three types of waveguide (from a SWG to a PPC taper and then from a PPC taper to a PPC waveguide). By judicious choice of the coupling parameters of the guided modes to the resonance, in principle high transmission can be achieved. It can be observed that the maximum transmission above 80% is not reduced excessively for a defect radius range of $0.578a$ (0.26877 μm) to $0.656a$ (0.30504 μm). A large range of defect radii is shown that is robust against manufacturing inaccuracies. In addition, when a light wave propagates to the output end of a PPC waveguide, as it traverses the defect, some of it is reflected and some of it is lost to the radiation modes in vacuum. Most of the rest propagates into the output end of the SWG. It should be emphasized that the values of the transmission spectra between point A and point B show a difference of only 3%, which again confirms that the introduction of localized defects within the two-step-size lattice constant PPC tapers can efficiently contain the transmitted light from emerging from the PPC waveguide to the z axis (shown in Fig. 1) and will result in a mode match that increases coupling efficiency and decreases reflection losses. Moreover, if the defect radius is controlled properly in the range $0.2a$–$0.33a$ at the entrance and exit terminals of the PPC tapers, the PPC circuit can be used as a good reflector.

The optimum relative position of the defect along both the x axis and the z axis has also been investigated. On the basis of our simulations, variations in the x axis indicate that the optimum position is $x = 0$ (Fig. 1), which corresponds to the mirror's symmetry axis. With respect to the position along z axis, Fig. 5 shows the normalized transmitted power obtained as a function of z/a at points A and B for a wavelength of incident light that corresponds to $\lambda = a/0.3 = 1.55$ μm, where the SWG's width is $w = 2.4$ μm, the defect radius is $r = 0.289$ μm, and z is the defect position. It can be seen that there is one z/a position that provides relative transmission maxima: $z_{opt} = 10.4a$. Setting a defect in one of the PPC tapers depicted in the inset of Fig. 5 indicates that the transmission is above 80% for a range of defect positions z from $0.981a$ to $10.57a$. That is, there can be a large range of tolerances of manufacturing inaccuracies for the defect position.

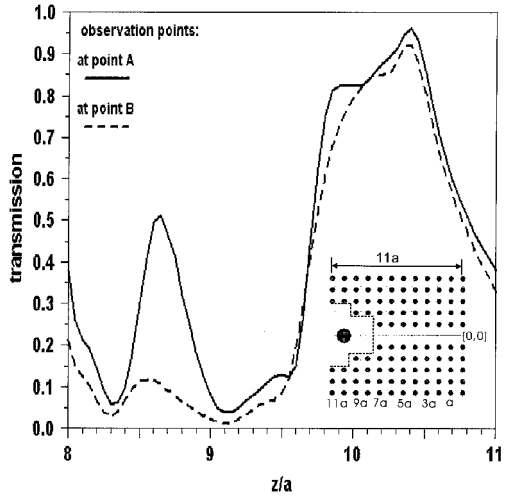

Fig. 5. Normalized transmitted power obtained as a function of z/a at points A and B for a wavelength of incident light corresponding to $\lambda = a/0.3 = 1.55$ μm, for SWG width $u = 2.4$ μm, defect radius $r = 0.289$ μm, and defect position z.

Figure 6 shows the steady state of the electric field (E_y) for input–output coupling for two cases: (a) conventional PPC tapers without defects [Fig. 6(a)] and two-step-size PPC tapers with optimum defects [$w = 2.4$ μm, $r = 0.289$ μm, and $z_{\text{opt}} = 10.4a$; Figs. 6(b)]. The wavelength of the incident light corresponds to $\lambda = a/0.3 = 1.55$ μm. The size of each image plane displayed is 30×10 μm. From the simulations we can observe that the shape of the PPC taper structure plays a critical role in changing the coupling efficiency between a conventional SWG and a PPC tapers, and thus we conclude that the two-step-size lattice constant PPC taper structure is superior to the other possible patterns of the PPC *taper,* particularly for our specified sample, i.e., silicon dielectric rods embedded in a silica medium, set in 2D square lattices. The electric field (E_y) distributions in the PPC waveguide with the conventional PPC taper structure but without defects are displayed in Fig. 6(a); a standing-wave pattern in the input SWG appears. The coupling loss comes from reflection at the junction between the SWG and the PPC taper; therefore some parts are propagated back to the input end of the SWG and some parts decay in the sides of the input end of the SWG. The field distributions exhibit a sinusoidal oscillation inside the PPC waveguide. When the light waves emerge from the output end of the PPC taper, little parts of them are coupled to the output end of the SWG and most of them decay exponentially in air. It can be clearly seen that the field distributions in the output end of the PPC taper, as shown in Fig. 6(a), are much weaker than those in the input end. In contrast, the field distributions inside the input end of the PPC taper are nearly the same as those in the output end, as shown in Fig. 6(b). These results confirm that designing appropriate PPC waveguide tapered structures that contain one pair of defect rods placed at optimal positions can significantly enhance coupling efficiency and depress reflection. Therefore it is expected that the tapered structures will support a favorable environment for establishing suitable field distributions, and the introduction of defect pairs can efficiently contain the light waves and form a new diffraction center of the light source (the scattering cross section results from a coherent superposition of individual amplitudes of light waves) in the cavity-like structures in the PPC taper region. Consequently, favorable coupling from the SWG through the PPC taper to the PPC waveguide is achieved when the optimal defect configuration is employed. Note that constructive interference in the input–output PPC tapers leads to increased coupling efficiency that is attributed mainly to the use of an optimal design defect configuration.

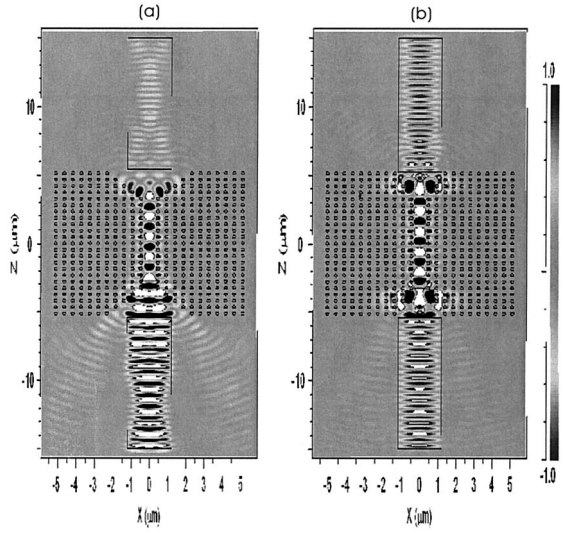

Fig. 6. Steady state of the electric field (E_y) for input–output coupling (a) with the conventional PPC tapers without defects and (b) with two-step-size PPC tapers with optimum defects ($w = 2.4$ μm, $r = 0.289$ μm, and $z_{opt} = 10.4a$). The wavelength of the incident light corresponds to $\lambda = a/0.3 = 1.55$ μm. The size of each image plane displayed is 30 μm $\times$ 10 μm.

Figure 7 shows the normalized transmission spectra of a 15-row PPC waveguide coupled to the entrance and exit terminals relative to a/λ for (1) a 0.5-μm width, two-step-size lattice constant PPC taper with a defect ($a/\lambda = 0.3$), (2) a 2.4-μm-width, two-step-size lattice constant PPC taper without a defect ($a/\lambda = 0.3$); (3) the same as case (2) except with a defect, (4) the same as case (3) except with $a/\lambda = 0.289$, and (5) the same as case (3) except with $a/\lambda = 0.306$. To obtain these results we launched an incident pulsed field at the input end of the SWG. The fundamental mode of the SWG was excited by a pulsed wave that propagates along the z direction (Fig. 1), and the transmission spectra field was calculated with the overlap integral between the launched and the measured fields at point B. The transmission spectra were calculated from the Fourier-transformed time series and normalized with respect to the launched pulse. In Fig. 7 the lower transmission presented in case (1) is due to the nar-

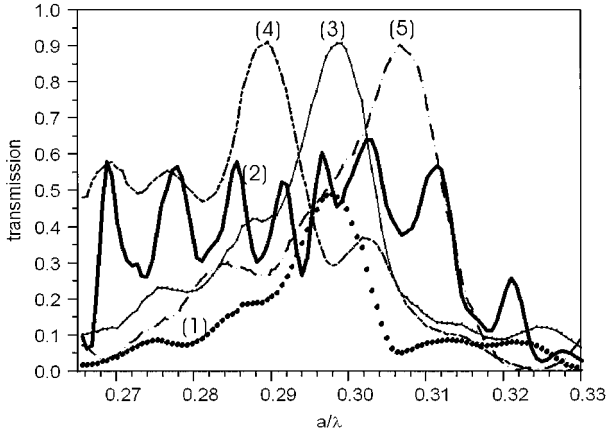

Fig. 7. Normalized transmission spectra of a 15-row PPC waveguide coupled to the entrance and exit terminals relative to a/λ for (1) a 0.5-μm width, two-step-size lattice constant PPC taper with a defect ($a/\lambda = 0.3$), (2) a 2.4 μm-width, two-step-size lattice constant PPC taper without a defect ($a/\lambda = 0.3$), (3) the same as case (2) except with a defect, (4) the same as case (3) except that $a/\lambda = 0.289$, and (5) the same as case (3) except that $a/\lambda = 0.306$.

rower width of SWG. The resonances that appear in the transmission spectrum of the PPC taper without a defect in case (2) are due to the Bragg reflection created by the mode mismatch at the interface between the SWG and the PPC tapers, and thus the number of resonances depends on the length of the PPC taper. When the proposed defect configuration is set, the response is sharply diminished because better mode matching at the interfaces of the PPC waveguide is achieved. According to case (3) of Fig. 7, an average transmission level larger than 80% is achieved for a normalized frequency range from $0.294(a/\lambda)$ to $0.302(a/\lambda)$, and the maximum transmission exceeds 90%, which enhances the 26.9% average transmission level achieved with the PPC taper without defects when the SWG's width is 2.4 μm. However, from Fig. 7 it can be observed that the bandwidth of case (3) is smaller, although it still satisfies bandwidth requirements for optical communications. One of the reasons for this is that a larger-sized defect radius ($r = 0.289$ μm) is used to achieve high coupling efficiency. That is, the high coupling efficiency is achieved with a trade-off of a bandwidth that becomes more sensitive to the normalized frequency employed to optimize the parameters of the defects. To illustrate this point we employed the same optimization procedure but for two different normalized frequencies, 0.289 (a/λ) and 0.306 (a/λ), as shown for cases (4) and (5) in Fig. 7. In case (5) for normalized frequency 0.306 (a/λ), the optimum defect configuration is obtained for $r_{opt} = 0.3$ μm and $z_{opt} = 10a$. It can be seen that in cases (3)–(5) the transmission spectra are shifted toward the normalized frequency employed in the optimization procedures. This means that the central frequency will be controlled for optical communications by determination of the optimal parameters of the defect configuration in PPC tapers.

4. Summary

In conclusion, we have reported a coupling technique based on setting localized defect pairs within PPC tapered structures at the two ends of a PPC waveguide in the form of a 2-D square lattice of dielectric rods in a silica medium. The coupling technique achieves mode matching at the input–output interface between SWG and PPC waveguides, reducing reflection losses and significantly improving transmission efficiency. Procedures to determine the best defect and waveguide parameters have been optimized to achieve highest transmission. The simulation results show that, by setting defect properly, one can achieve a better than 90% transmission at a standard optical communication wavelength of 1.55 μm, which sharply enhances the transmission obtained when no defects are considered. The technique is robust against manufacturing inaccuracies and is valid for both coupling into and out of a photonic crystal waveguide. Finally, its is worth mentioning that one can control the central frequency by determining this defect configuration by using the optimization procedure. In addition, the proposed structure can act as a good reflector when the range of a defect radius is properly adjusted.

The authors acknowledge financial support from the National Science Council of the Republic of China through grant NSC92-2112-M-009-023.

References and Notes

1. T. F. Krauss, R. M. De La Rue and S. Brand, "Two-dimensional photonic-bandgap structures operating at near-infrared wavelength," Nature **383,** 699–702 (1996).
2. L.-L. Lin and Z.-Y. Li, "Sensitivity to termination morphology of light coupling in photonic-crystal waveguides," Phys. Rev. B **69,** 193103 (2004).
3. M. E. Potter and R. W. Ziolkowski, "Two compact structures for perpendicular coupling of optical signals between dielectric and photonic crystal waveguides," Opt. Express **10,** 691 (2002), http://www.opticsexpress.org.
4. Y. Xu, R. Lee, and A. Yariv, "Adiabatic coupling between conventional dielectric waveguides and waveguides with discrete translational symmetry," Opt. Lett. **25,** 755–757 (2000).
5. A. Mekis and J. D. Joannopoulos, "Tapered couplers for efficient interfacing between dielectric and photonic crystal waveguides," IEEE J. Lightwave Technol. **19,** 861–865 (2001).
6. T. D. Happ, M. Kamp, and A. Forchel, "Photonic crystal tapers for ultracompact mode conversion," Opt. Lett. **26,** 1102–1104 (2001).
7. P. Sanchis, J. Marti, J. Blasco, A. Martinez, and A. Garcia, "Mode matching technique for highly efficient coupling between dielectric waveguides and planar photonic crystal circuits," Opt. Express **10,** 1391–1397 (2002), http://www.opticsexpress.org.
8. J. Jiang, J. Cai, G. P. Nordin, and L. Li, "Parallel microgenetic algorithm design for photonic crystal and waveguide structures," Opt. Lett. **28,** 2381–2383 (2003).
9. P. Sanchis, J. Marti, A. Garcia, A. Martinez, and J. Blasco, "High efficiency coupling technique for planar photonic crystal waveguides," Electron. Lett. **38,** 961–962 (2002).
10. A. Mekis, J. C. Chen, I. Kurland, S. Fan, P. R. Villeneuve, and J. D. Joannopoulos, "High transmission through sharp bends in photonic crystal waveguides," Phys. Rev. Lett. **77,** 3787–3790 (1996).

11. S.-Y. Lin, E. Chow, V. Hietala, P. R. Villeneuve, and J. D. Joannopoulos, "Experimental demonstration of guiding and bending of electromagnetic waves in a photonic crystal," Science **282,** 274–276 (1998).
12. See http://ab-initio.mit.ed/mpb.
13. S. G. Johnson and J. D. Joannopoulos, "Block-iterative frequency-domain methods for Maxwell's equations in a plane-wave basis," Opt. Express **8,** 173–190 (2001), http://www.opticsexpress.org.
14. M. Bayindir, B. Temelkuran, and E. Ozbay, "Tight-binding description of the coupled defect modes in three-dimensional photonic crystals," Phys. Rev. Lett. **84,** 2140–2143 (2000).
15. T. J. Karle, D. H. Brown, R. Wilson, M. Steer, and T. E. Karuss, "Photonic crystal light deflection devices using the superprism effect," IEEE J. Sel. Top. Quantum Electron. **8,** 909–918 (2002).
16. Y. Xu, R. Lee, and A. Yariv, "Adiabatic coupling between conventional dielectric waveguides and waveguides with discrete translational symmetry," Opt. Lett. **25,** 755–757 (2000).
17. A. Taflove, *Computational Electrodynamics* (Artech House, Norwood, Mass., 1995).
18. J. P. Berenger, "A perfectly matched layer for the absorbing boundary condition," J. Comput. Phys. **114,** 185–200 (1994).